Materials and Design 92 (2016) 184–188

Contents lists available at ScienceDirect

Materials and Design

journal homepage: www.elsevier.com/locate/matdes

Study by DSC and HRTEM of the aging strengthening of Cu–Ni–Zn–Al alloys

M.J. Diánez [b], E. Donoso [a], J.M. Criado [b,*], M.J. Sayagués [b], G. Díaz [a], L. Olivares [c]

[a] Departamento de Ciencia de los Materiales, Facultad de Ciencias Físicas y Matemáticas, Universidad de Chile, Casilla, 2777 Santiago, Chile
[b] Instituto de Ciencias de Materiales de Sevilla, C.S.I.C., Centro Mixto Universidad de Sevilla—C.S.I.C., Américo Vespucio 49, Isla de la Cartuja, 41092 Sevilla, Spain
[c] Departamento de Materiales Nucleares, Comisión Chilena de Energía Nuclear, CCHEN, Amunategui 95, Santiago, Chile

ARTICLE INFO

Article history:
Received 13 May 2015
Received in revised form 23 November 2015
Accepted 7 December 2015
Available online 9 December 2015

Keywords:
Cu–Ni–Zn and Cu–Ni–Zn–Al alloys
Calorimetry
Precipitation hardening

ABSTRACT

The structural changes of a Cu–12 wt.% Ni–17 wt.% Zn–1.7 wt.% Al alloy as a function of the aging temperature have been studied by means of Differential Scanning Calorimetry (DSC), high resolution transmission electron microscopy (HRTEM) and hardness measurements. It has been proposed a hardening mechanism that implies the crystallization of a Ll_0 Cu_2NiZn phase coherent with the matrix α phase followed, firstly, by its transformation into a Ll_2 coherent phase and, secondly, by the precipitation of this phase. It has been shown that aluminum play an important role in the precipitation hardening process because Cu_2NiZn precipitates are not formed by aging a ternary Cu–Ni–Zn alloy of similar composition. It has been shown by the first time that DSC could be a powerful tool for discriminating the whole set of phase transformations undergone by alloys as a function of the annealing temperature from a single heating run.

1. Introduction

Copper is the most promising material for those industrial applications that require materials with a high electrical and/or thermal conductivity, although it is necessary to improve the mechanical properties and corrosion resistance of copper [1–3]. Cu–Ni–Zn alloys, known as "nickel silver" have a great wear and corrosion resistance and, therefore, they are excellent candidates for the above applications [4,5]. Nickel improves the mechanical properties of these alloys, while zinc lowers the melting point and minimizes the porosity [5]. A single copper α phase would be formed for zinc weight percentages lower than 35% at temperatures lower than 427 °C, according to the ternary Cu–Ni–Zn diagrams reported in literature [6]. It has been shown that the mechanical properties of Cu–26Ni–17Zn [4,5] and Cu–10Ni–20Zn [3,7], both in the composition range of the α copper phase, are improved by cold rolling strengthening, but, unfortunately, with the handicap of a fall of their electrical conductivity [3]. However, both the tensile strength and the electrical conductivity are simultaneously improved if the strengthening is achieved by precipitation hardening instead of by cold rolling [3]. This behavior explains that a high motivation has arisen for the study of the strengthening of alloys by precipitation hardening [8–19].

Zhou et al. [7] have reported in a recent paper that the precipitation hardening of Cu–Ni–Zn alloys can be attained by adding a small percentage of a fourth element like aluminum. They have concluded that the mechanical properties of Cu–10Ni–20Zn–1.2Al are dramatically improved by aging this alloy at 500 °C due to the formation of nanosized precipitates with the $L1_2$ type ordered structure. However, a study of the mechanism of formation of the precipitates as a function of the aging temperature is still missing. The scope of this paper is to study the evolution of the microstructure of a Cu–Ni–Zn and a Cu–Ni–Zn–Al alloy of closed composition as a function of the aging temperature. Differential Scanning Calorimetry (DSC) could be a proper tool for discerning the transformations undergone by the alloys as a function of the annealing temperature because it could allows discriminate the thermal effects associated to these transformations. X-ray diffraction (XRD), microhardness measurements and High Resolution Transmission Electron Microscopy (HRTEM) have been combined with DSC for analyzing the microstructure evolution as a function of the temperature.

2. Experimental method

The alloys were prepared by melting stoichiometric mixtures of electrolytic copper (99.95% purity), nickel, zinc and aluminum of high purity in an induction furnace under argon atmosphere. The ingots were annealed at 1123 K during 24 h to achieve complete homogenization before cooling down to room temperature. Subsequently, the material was submitted to successive cold-rolling treatments with intermediate annealing of 1 h at 1123 K until reaching a thickness of 3 mm. After the last annealing treatment the material was water quenched for preserving the α-Cu structure of the homogeneous supersaturated solid solution. The weight percentage compositions determined from chemical analysis for the two samples here prepared are

* Corresponding author.
E-mail address: jmcriado@icmse.csic.es (J.M. Criado).

http://dx.doi.org/10.1016/j.matdes.2015.12.030
0264-1275/

Cu–10.9Ni–19.9Zn (Cu–11Ni–20Zn here after) and Cu–12Ni–17Zn–1.7Al, respectively. These compositions correspond, respectively to the following fractional atomic compositions: $Cu_{0.675}Ni_{0.115}Zn_{0.210}$ and $Cu_{0.676}Ni_{0.126}Zn_{0.159}Al_{0.039}$.

The X-ray diffractions diagrams (XRD) were recorded with a PHILPS X'pert Pro equipped with an X'celerator detector and a graphite diffracted beam monochromator. CuKα radiation and a nickel filter were used. A voltage of 40 kV and an intensity of 40 mA were employed. The lattice parameters were determined from the XRD peaks by means of least-squares fitting using the CellRef program.

A DSC TA Instruments, model Q10 was used. The DSC diagrams were recorded under an argon flow (10^{-4} m^3 min^{-1}) from room temperature up to the maximum temperature allowed by the equipment (993 K), although only the temperature range in which peaks are observed will be considered for plotting the DSC diagrams. A high-purity well-annealed copper disk was used as reference material in order to minimize the base line deviation. The base line was obtained using annealed copper both as reference and sample material under the same experimental conditions used for recording the DSC curve to be corrected.

High resolution transmission electron microscope (HRTEM) images were done in a 300 kV TECNAI G2 F30 microscope with a field emission system (point resolution 0.2 nm). The measurements of the HRTEM images were done with the Digital Micrograph software (Gatan Inc.). The specimens for HRTEM observation were prepared by cutting disks of 3 mm in diameter from the sample sheets. The disks were thinned until half a micron by dimple and ion milling techniques.

Vickers microhardness measurements were performed at room temperature in a high accuracy Duramin −1/−2 Struers machine employing a load of 1.96 N during 10 s on specimen disks. Each microhardness value was calculated as an average of 10 microhardness indentations, with a standard deviation of approximately 2%.

3. Results and discussion

The XRD patterns of the samples Cu–11Ni–20Zn and Cu–12Ni–17Zn–1.7Al are shown in Fig. 1. The lattice parameters obtained are equal to $a = 3.6481 \pm 0.0013$ nm and $a = 3.6478 \pm 0.0022$ nm, respectively. These values roughly agree with those to be expected for Cu–Ni–Zn α phase in the copper rich region of the ternary phase diagram according with the expression $a\ (\mathrm{nm}) = 0.3608 + 0.021\ x_{Zn} - 0.011\ x_{Ni}$, proposed for fractional atomic composition in the range: $x_{Zn} < 0.23$, $x_{Ni} < 0.33$ [20]. These results supports that the two alloys here prepared have a homogeneous composition and are constituted by a single phase isostructural with copper.

Fig. 2 shows the DSC diagram for the Cu–11Ni–20 Zn alloy with two exothermic peaks at 373 K and 442 K as obtained at a heating rate of 20 K/min. The exothermic character of the DSC peaks can be understood taking into account the extra energy stored by the starting alloy since

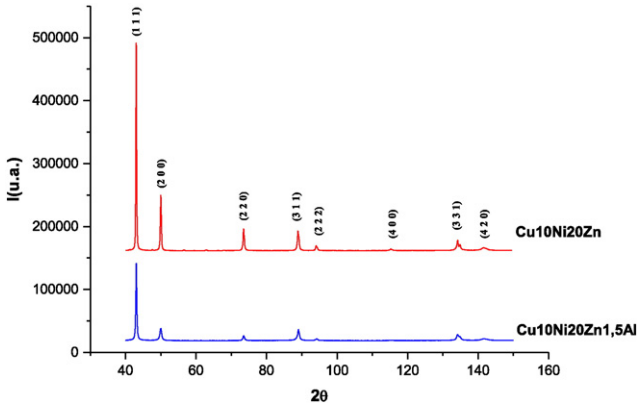

Fig. 1. XRD diagrams of Cu–11Ni–20Zn and Cu–12Ni–17Zn–1.7Al alloys.

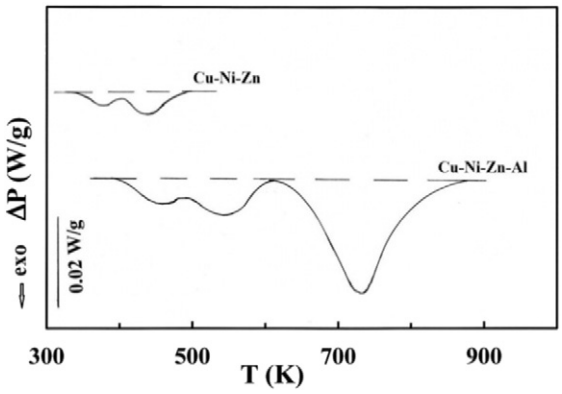

Fig. 2. DSC curves recorded at a heating rate of 0.333 $K \cdot s^{-1}$ of the Cu–11Ni–20Zn and Cu–12Ni–17Zn–1.7Al samples previously quenched from 1123 K.

it is a supersaturated solid solution far from the thermodynamic equilibrium. This extra energy is lost as the alloy is approaching to the equilibrium with increasing temperature. To explain the results shown in Fig. 2 it would be necessary to bear in mind that the isothermal sections of the ternary Cu–Ni–Zn phase diagram points out the formation of a Cu_2NiZn phase in equilibrium with the copper α phase at temperatures lower than 427 °C [21]. The structural changes undergone by Cu_2NiZn as a function of the temperature can be understood by dividing the *fcc* structure into four interpenetrating simple cubic lattices [6,22–23] with the following coordinates: I (0,0,0), II (½,½,0), III (½,0,½) and IV (0,½,½). These lattice positions are occupied by Zn, Ni, Cu and Cu, respectively, in the fully ordered Ll_0 phase (AuCu type) that is stable up to 600 K [6, 22] at which it is transformed into the partially ordered Ll_2 phase ($Au–Cu_3$ type) with the Zn atoms positioned at the corner of the cube while Cu and Ni are randomly distributed into the sublattices II, III and IV. The Ll_0 Cu_2NiZn phase transforms at 1200 K into an fcc disordered structure with Zn, Ni and copper randomly distributed at the corners and the center of the cube faces. On the other hand, Simak et al. [24], from first principle Montecarlo calculations, have predicted the existence of partially ordered Ll_0 phase with Zn and the half of the Cu atoms placed at the cube corner and Ni and the other half of Cu placed at the center of the cube faces. This phase would be stable between 850 and 1200 K according with Simak et al. calculations, but experimental evidence has not been yet reported. It must be pointed out that the temperatures for the $Ll_0 \rightarrow Ll_1$ transitions can be significantly modified by small variations of the Cu_2NiZn stoichiometric composition. Thus, the cross section of the phase diagram for the composition $Cu_{0.5}Ni_{0.5-x}Zn_x$ ($0.15 < x < 0.35$) clearly points out that the temperature of the $Ll_0 \rightarrow Ll_1$ phase transition reach a maximum for a value of $x = 0.25$ that correspond to the fractional atomic composition of the Cu_2NiZn [25]. This transition temperature dramatically decreases either increasing or decreasing the value of x [25]. It must be pointed out that in most of the cases the phase diagrams have been calculated from the measurement of physical properties like electrical conductivity [25]. The structures of the different Cu_2NiZn phases are too closed for being discriminated from X-ray diffraction or HRTEM, but their crystalline structures were discerned by neutron diffraction [22,23].

Taking into account the above considerations the first DSC peak of Fig. 2 could be attributed to the formation of a Ll_0 phase from the α phase of the supersaturated Cu–11 Ni–20 Zn, while the second DSC peak shown in Fig. 2 could be associated to the $Ll_0 \rightarrow Ll_1$ phase transition. A TEM-HRTEM analysis has been carried out in order to check if Cu_2NiZn has been generated during the annealing of the Cu–11Ni–20Zn alloy. Fig. 3 shows a HRTEM picture taken for the Cu–11Ni–20Zn sample annealed for 4 h at the temperature of 430 K corresponding to its second DSC peaks in Fig. 2. This picture points out the formation of nanocrystals (about 5 nm) of a new phase embedded in the (111) planes of α copper framework. Unfortunately, the too small size of the crystals has not

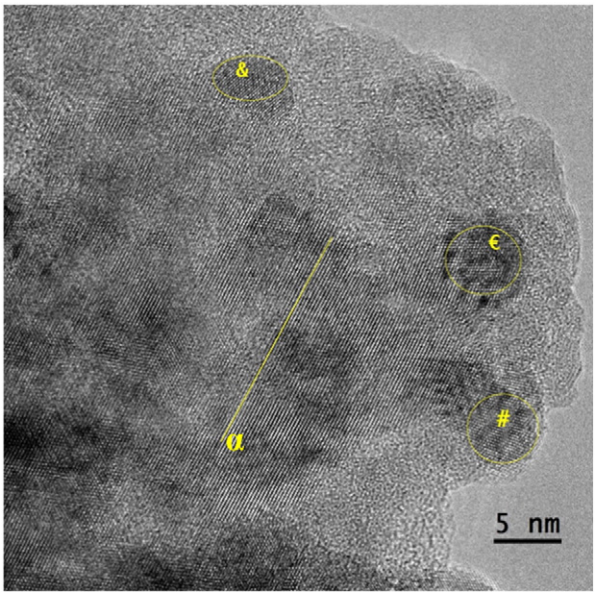

Fig. 3. HRTEM image of Cu–11Ni–20Zn annealed at 430 K showing nanocrystals (≈5 nm) of the Cu_2NiZn coherent phase embedded in the (110) planes of the α phase. The measured interplanar spaces, d, are shown. (€) Cu_2NiZn [111] zone axis; (&) Cu_2NiZn (200) planes (d = 0.20 nm); (#) Cu_2NiZn (111) planes (d = 0.18 nm); (α) α copper (110) planes (d = 0.25 nm).

allowed determining the composition by EDAX, but the interplanar distances, d, determined by HRTEM match the values corresponding to the Cu_2NiZn phase. Moreover, the segregation of other binary phases is not thermodynamically favored provided that Cu–Ni, Cu–Zn and Ni–Zn are miscible all over the composition range according to the phase diagrams of the Cu–Ni–Zn system. These results support that Cu_2NiZn nanocrystals coherent with the starting alloy have been formed. The HRTEM image in Fig. 3 supports that the (111) and (200) planes of Cu_2NiZn nanocrystals are embedded into the (110) planes of the framework α phase.

The DSC diagram of the Cu–12Ni–17Zn–1.7Al alloy recorded at a heating rate of 20 K/min is shown in Fig. 2 together with the previously obtained for the Cu–11Ni–20Zn sample. These results shows that in the case of the quaternary alloy a third strongly exothermic peak appears at about 723 K besides the two overlapping peaks similar to those previously observed in the DSC diagram of the ternary alloy. However, Fig. 2 shows that the temperatures of these two peaks are about 100 K higher than the corresponding ones to the Cu–11Ni–20Zn alloy, which suggests that the small percentage of aluminum added clearly improves the stability of the starting α phase of the alloy. Currently there are not thermodynamic data that support this behavior because to our knowledge the phase diagram of the Cu–Ni–Zn–Al quaternary alloy is not available. However, it would be tentatively explained by assuming the association of aluminum to copper in short range order (SRO) regions [26,27] that could hinder the diffusion of copper, displacing the formation of the Ll_2 phase at higher temperatures. It must be pointed out that the finding of the influence of aluminum on the stabilization of the structure of the starting solid solution, here reported by the first time, was made possible by the use of DSC. This is because this method allows discerning the temperature ranges at which successive phase transitions occurs from a single rising temperature run. A study by HRTEM would help to understand the textural and structural changes undergone by the sample during the annealing at different temperatures.

Fig. 4 shows the TEM-HRTEM micrographs of the Cu–12Ni–17Zn–1.7Al annealed during 4 h at 523 K, closed to the temperature shown in Fig. 2 for the second DSC peak of this alloy. Fig. 4b shows the formation of nanocrystal of a coherent phase embedded into the α phase matrix. The similarity between the DSC diagrams of the Cu–11Ni–20Zn and Cu–12Ni–17Zn–1.7Al alloys at temperatures lower than 550 K supports that this DSC peaks is associated to the formation of a coherent phase of Cu_2NiZn oriented along the planes (111) and (200). On the other hand, the TEM image shown in Fig. 4a points out that a large amount of dislocations have been generated at the time of the formation of the new phase from the Cu–12Ni–17Zn–1.7Al alloy. This effect has been promoted by the addition of a small percentage of aluminum to the ternary alloy, because dislocations were not observed on the Cu–11Ni–20Zn sample.

Finally, Fig. 5 includes the TEM-HRTEM images obtained for the Cu–12Ni–17Zn–1.7Al annealed for 3 h at 723 K that is inside the temperature range of the third large endothermic peak shown in Fig. 2. It is observed that a large number of very small Cu_2NiZn crystals (2–5 nm) have been segregated from the matrix. The fact that the crystal size of these precipitates were noticeably lower than the one reported by Zhou et al. [3,7] could be understood taking into account that the TEM pictures reported by these authors were obtained from samples annealed at 773 K instead of 723 K like here and it would be expected an exponential increase of the crystal growth rate with the temperature. Moreover, it is noteworthy to remark that the XRD profiles recorded by us for the annealed samples were quite similar to the XRD diagram of the starting sample shown in Fig. 1 and have not been included for the sake of the brevity. This fact clearly shows that only the diffraction peaks corresponding to the matrix alloy were observed in the annealed samples. This behavior could be understood considering that, firstly, the low concentration expected for the new Ll_2 phase and, secondly, the extremely high broadening of the diffraction peaks associated to the nanosized crystals formed would make difficult discriminating the new phase formed from XRD profiles.

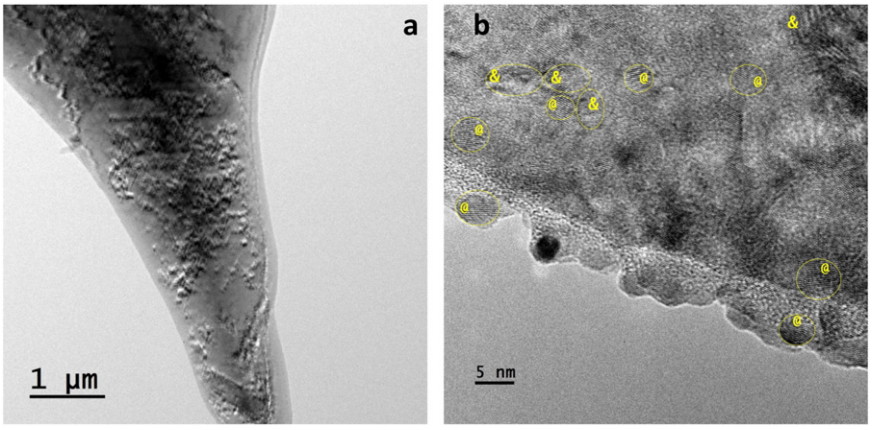

Fig. 4. Transmission electron micrographs of Cu–12Ni–17Zn–1.7Al annealed at 523 K. (a) Details of dislocations as shown by TEM; (b) HRTEM image showing nanocrystals (2–5 nm) of the Cu_2NiZn coherent phase including the measured interplanar spaces, d,: (&) Cu_2NiZn (200) planes (d = 0.20 nm); (@) Cu_2NiZn (110) planes (d = 0.25 nm).

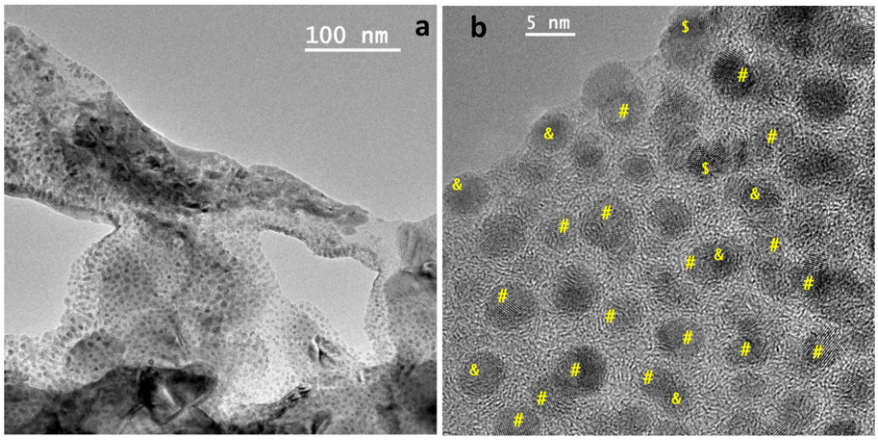

Fig. 5. Transmission electron micrographs of Cu–12Ni–17Zn–1.7Al annealed at 723 K. (a) Formation of very small precipitates as shown by TEM. (b) HRTEM image where different interplanar spaces of the Cu_2NiZn monocrystalline phase were measured: ($) Cu_2NiZn [110] zone axis; (&) Cu_2NiZn (200) planes (d = 0.20 nm); (#) Cu_2NiZn (111) planes (d = 0.18 nm).

The formation of precipitates in the quaternary alloy would be explained by assuming that the dislocations formed in the previous step interact with the crystals of the coherent Ll_2 phase embedded into the matrix whose stability is not sustained by increasing the temperature leading to the precipitation from the surrounding matrix [28]. The above results are supported by those previously reported by Zhou et al. [7]. These authors found that the precipitation of nanocrystals by annealing a Cu–10Ni–20Zn–1.6Al (wt.%) sample at 773 K was associated to an increase of the alloy hardness. However, the study of the evolution of the alloys structure as a function of the annealing temperature here developed was still missing.

The DSC and HRTEM results above reported would support a Cu_2NiZn precipitation mechanism from Cu–12Ni–17Zn–1.7Al that implies the following three steps: 1) the crystallization of a coherent Ll_0 Cu_2NiZn phase embedded into the α matrix phase, pointed out by the first DSC peak at 463 K; 2) the $Ll_0 \rightarrow Ll_2$ phase transformation, marked by the second DSC peak at 550 K and 3) the precipitation of the Ll_2 phase responsible of the third DSC peak at 723 K. It is clear that the addition of a small amount of aluminum exerts an important role in the precipitation of the Cu_2NiZn, provided that we have not observed the formation of precipitates in the Cu–11Ni–20Zn ternary alloy.

Taking into account the application of these alloys, it would be of great interest to study the influence of the structural changes previously reported on their mechanical properties. The analysis of the variation of the Vickers microhardness as a function of the annealing time at different temperatures has been used for this purpose. The hardness measurements of the samples previously aged at different temperatures and times have been carried out at room temperature following the procedure described in the experimental section. Fig. 6 shows the variation of hardness of Cu–11Ni–20Zn versus aging time at 430 K. The hardness of Cu–12Ni–17Zn–1.7Al as a function of the aging times measured at 430, 520 and 720 K, respectively, are also included in Fig. 6 for a comparison. It is noteworthy to point out that the value of 131 HV here obtained for the hardness of the annealed Cu–12Ni–17 Zn–1.7Al sample prepared by quenching almost doubles the value previously reported by Zhou et al. [3]. This behavior could be understood bearing in mind that the load applied by Zhou et al. for determining the Vickers hardness was ten times higher than the applied here. Thus, the value reported in reference [3] could be representative of the bulk hardness, while the one here reported could be closer to the surface hardness and one would expect that the concentration of lattice defects is higher on the surface of quenched samples than into their bulk.

It is shown in Fig. 6 that the hardness of the Cu–11Ni–20Zn is independent of the aging time. This fact indicates that the formation of the Ll_2 coherent phase into the alloy matrix (see Fig. 3) does not improve the mechanical properties of this alloy. This behavior could be understood taking into account that the energy stored by the grain boundaries, represented by the border line between the matrix and the embedded coherent Ll_2 phase crystals, is very low and their strengthening ability is rather weak [28]. The lack of influence of the aging time at 430 K on the hardness of Cu–12Ni–17Zn–1.7Al (Fig. 6) supports the above conclusion. On the other hand, the weak dependence of the hardness of the Cu–12Ni–17Zn–1.7Al alloy from the aging time at 520 K (Fig. 6) could be exclusively attributed to the dislocations generated by the annealing at this temperatures as shown in Fig. 4a. No hardening response would be expected from the grain boundaries constituting the border line between the coherent Ll_2 phase and the matrix, provided the low energy that they store [28]. The grain boundaries are penetrable by moving dislocations, contrarily what happens with the precipitates that are impenetrable obstacles to dislocation movements, leading to an improvement of the mechanical properties of the alloy [28,29].

Finally, Fig. 6 shows that the Vickers hardness of the Cu–12Ni–17Zn–1.7Al alloy noticeably increases as a function of the aging time at 700 K until reaching a maximum value of 190 HV after about 200 min of annealing and slowly decreases thereafter. The fact that a maximum is reached indicates that a precipitation equilibrium is attained. This behavior has been commonly found by studying the precipitation hardening of alloys [7,17] and have been attributed to the growth of the precipitates until reaching a critical value at which the hardness reach a maximum, beyond which it decreases with aging time [17,29]. It has

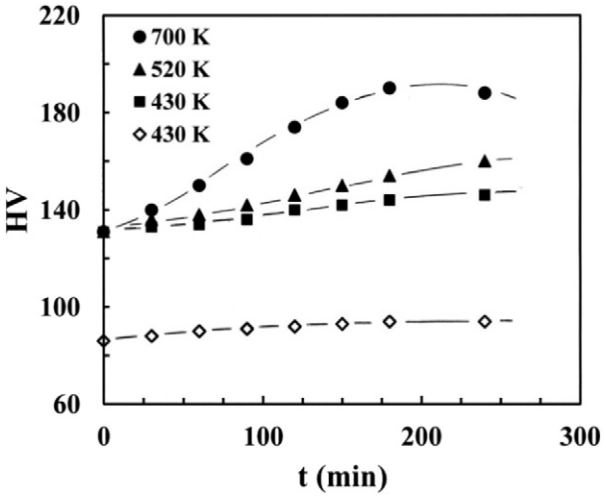

Fig. 6. Vickers microhardness vs. time for different aging temperatures (samples previously quenched from 1123 K). (◇) Cu–11Ni–20Zn, (●, ▲, ■) Cu–12Ni–17Zn–1.7Al.

been shown [17] that the value of the hardness at the maximum is almost independent of the aging temperature, which would explain that the value of Hv at the maximum of the Hv versus aging time plot obtained by us matches the corresponding one attained by Zhou et al. [3,7]. It must be considered that the lattice defects distribution between the bulk and the surface of the alloy would be approached as far as the annealing time is in progress, leading to a progressive agreement between bulk and surface hardness measurements. In summary, the results here reported clearly show that the hardening by annealing of the Cu–12Ni–17Zn–1.7Al quaternary alloy takes place at the temperature range at which the nanophase precipitation takes place, but the formation of a Ll_2 coherent phase embedded into the framework phase does not influence the hardness of the alloy. This explains that the annealing of the Cu–11Ni–20Zn ternary phase does not appreciably alter the hardness of the sample.

4. Conclusions

It has been shown that DSC is a powerful tool for discriminating the successive transformations undergone by an alloy as a function of the temperature from a single run obtained under linear rising temperature. The analysis of HRTEM observations combined with DSC and microhardness measurements supports the proposal of a mechanism for the precipitation hardening of Cu–12Ni–17Zn–1.7Al that implies the following three steps: 1) Formation of nanocrystals of a Ll_0 coherent phase of Cu_2NiZn; 2) Transformation of this phase into a Ll_2 coherent phase after annealing the sample at the proper temperature and 3) Precipitation of the Ll_2 phase by growing of the nuclei previously formed in the steep 2 if the annealing temperature continues in progress. These results together with those obtained from the microstructural study of a Cu–11Ni–20Zn allow concluding that the coherent nanocrystal embedded in the matrix alloy exhibits no age hardening response. The age hardening response is near exclusively due to the formation of precipitates induced by the addition of aluminum to Cu–Ni–Zn alloys.

Acknowledgments

The authors would like to acknowledge the Fondo Nacional de Desarrollo Científico y Tecnológico (FONDECYT) for financial support, Project N° 1140782. It is also greatly appreciated the facilities provided by the Instituto de Ciencias de Materiales de Sevilla (Spain) and the Departamento de Ciencia de los Materiales, Facultad de Ciencias Físicas y Matemáticas, Universidad de Chile (Chile) and the Departamento de Materiales Nucleares de la Comisión Chilena de Energía Nuclear (Chile).

References

[1] J.R. Groza, J.C. Gibeling, Mater. Sci. Eng. A 171 (1993) 115–125.
[2] R.H. Palma, A. Sepúlveda, R. Espinoza, A. Zúñiga, M.J. Diánez, J.M. Criado, M.J. Sayagués, Mater. Sci. Eng. A 384 (2004) 262–269.
[3] X.Z. Zhou, Y.C. Su, J.M. Sun, J. Mater. Sci. 45 (2010) 3080–3087.
[4] S. Nagarjuna, B. Gopalakrishna, M. Srinivas, Mater. Sci. Eng. A 429 (2006) 169–172.
[5] S. Nagarjuna, M. Srinivas, K.K. Sharma, Acta Mater. 48 (2000) 1807–1813.
[6] N. Lebrun, P. Perrot, Non-ferrous metal systems, Part 3, Landolt–Börnstein-Group IV Physical Chemistry, vol. 11C3, Springer, Stuggart, Germany 2007, pp. 338–354.
[7] X.Z. Zhou, Y.C. Su, Mater. Sci. Eng. A 527 (2010) 5153–5156.
[8] J. Ruzik, J. Stasic, V. Rajkovic, D. Bozik, Mater. Des. 49 (2013) 746–754.
[9] W.H. Zhou, H. Guo, Z.J. Xie, C.J. Shang, R.D.K. Misra, Mater. Des. 63 (2014) 42–49.
[10] X.P. Ding, H. Cui, J.X. Zhang, H.X. Li, M.X. Guo, Z. Lin, Mater. Des. 65 (2015) 1229–1235.
[11] B. Mirzhakani, Y. Payandeh, Mater. Des. 68 (2015) 127–133.
[12] P. Jiang, Y.D. Yu, G.S. Song, D. Liang, M. Kellan, M. Dollan, Mater. Des. 63 (2014) 136–141.
[13] X.Y. Liu, Q.L. Pan, X.L. Zhang, S.X. Liang, L.Y. Zzheng, F. Gao, H.L. Xie, Mater. Des. 58 (2014) 247–251.
[14] S. Sheibani, S. Heshmati-Manesh, A. Ataie, A. Caballero, J.M. Criado, J. Alloys Compd. 587 (2014) 670–676.
[15] S. Sheibani, A. Ataie, S. Heshmati-Manesh, A. Caballero, J.M. Criado, Thermochim. Acta 526 (2011) 222–228.
[16] E. Donoso, M.J. Diánez, J.M. Criado, Rev. Metal. 48 (2012) 67–75.
[17] E. Donoso, R. Espinoza, M.J. Diánez, J.M. Criado, Mater. Sci. Eng. A 556 (2012) 612–616.
[18] R.H. Palma, A. Sepúlveda, R. Espinoza, M.J. Diánez, J.M. Criado, M.J. Sayagués, Mater. Sci. Eng. A 391 (2005) 60–65.
[19] A. Varschavsky, E. Donoso, Mater. Sci. Eng. A 251 (1998) 208–215.
[20] G.A. Chadswick, B.B. Argent, J. Inst. Met. 88 (1960) 3418–3419.
[21] A. de Rooy, P.M. Bronsveld, J.T.M. de Hoson, Z. Metallkd. 73 (1982) 610–615.
[22] M. Hirabayashi, S. Hoshino, K. Sato, J. Phys. Soc. Jpn. 20 (1965) 381–388.
[23] G. Van der Weegen, R. Helmholdt, P. Bronsweld, J. de Hosson, Z. Metallkd. 74 (1983) 592–597.
[24] S.I. Simak, A.V. Ruban, I.A. Abrikosov, H.L. Skriver, B. Johansson, Phys. Rev. Lett. 81 (1998) 188–191.
[25] A. de Rooy, G.J.L. Van der Weegen, P.M. Bronsveld, J.T.M. de Hosson, Scr. Metall. 15 (1981) 1359–1364.
[26] A. Varschavsky, E. Donoso, Mater. Sci. Eng. A 145 (1991) 95–107.
[27] E. Donoso, A. Varschavsky, Mater. Sci. Eng. A 369 (2004) 10–15.
[28] K. Lu, K. Lu, S. Suresh, Science 324 (2009) 349–352.
[29] S.A. Lockier, F.W. Noble, J. Mater. Sci. 29 (1994) 218–226.